Journal of Polymer Research (2019) 26:205
https://doi.org/10.1007/s10965-019-1854-x

ORIGINAL PAPER

# Application of multiple regression analysis in optimization of metronidazole-chitosan nanoparticles

Hazem Abdul Kader Sabbagh[1] · Zead Abudayeh[1] · Suha Mujahed Abudoleh[1] · Jamal Alyousef Alkrad[1] · Mohd Zobir Hussein[2] · Samer Hasan Hussein-Al-Ali[1]

Received: 15 January 2019 / Accepted: 11 July 2019


## Abstract

The current work aims to developing MET-CSNPs nanocomposites as drug delivery system. The nanocomposites were prepared by ionic interactions method and optimized using multiple regression analysis. Independent variables included chitosan concentration (CS), tri poly phosphate concentration (TPP) and metronidazole concentration (MET); while dependent variables were percentage loading drug (LE), zeta potential and zeta size. Prepared nanocomposites were characterized by X-ray diffraction (XRD), Fourier-transform infrared spectroscopy (FTIR), thermal gravimetric analysis (TGA), scanning electron microscope (SEM) and in vitro drug release studies. TGA, FTIR and XRD studies indicated the presence of drug into final nanocomposites. In vitro drug release from nanocomposites was carried out and showed that the release rate of MET from the MET-CSNPs nanocomposites was very slow. These results indicate extended release of the drug from its respective nanocomposites, and therefore these nanocomposites have good potential to be used as extended-release formulation of the drugs.

**Keywords** Metronidazole · Chitosan nanoparticles · Multiple regression analysis · Optimization

## Introduction

Recently, the identification of the unique properties of nanoparticles has allowed their application in many fields such as drug and gene delivery [1, 2], biomedicine [3–5], tumor detection [6] and tumor treatment [7], this is due to their unique properties of small size, large surface area to volume ratio, stability over high temperatures, carrier the drugs into the cells and high reactivity to the living cells.

Extended-release formulations are the way for administration of drugs to be given as a single dose rather than as multiple doses. In this way, drug release can be completed over long periods of time, leading to constant level of the drug in the bloodstream. In addition, extended-release formulations increase the clinical efficacy of drugs. The preparation of drug nanocomposites as extended-release carriers has produces a burst in drug delivery systems in the field of pharmaceutical technology. Chitosan is widely used for this purpose because of their unique properties, such as ease of preparation, low cost, good biocompatibility, low cytotoxicity, and full protection of the drugs loaded [8–10].

Chitin is one of the most abundant natural polymers of all polysaccharides. One source of chitin is the outer crusts of lobsters and shrimp where chitin can easily be converted to chitosan [11, 12].

Chitosan (Poly-b-(1,4)-2-Amino-2-deoxy-D-glucose) is produced by deacetylation of chitin and can be formed from co-polymers of N-acetyl glucosamine and glucosamine. Chitosan can function as a viscosity-increasing agent, a coating agent, a mucoadhesive, a disintegrant, a film-forming agent and a tablet binder [13–16].

Chitosan can be considered one of the most important polymers in the pharmaceutical industry [17]. Natural polymer-based nanoparticles show an improvement on traditional oral method of drug delivery system in terms of efficiency and effectiveness [18].

✉ Samer Hasan Hussein-Al-Ali
samer.alali@iu.edu.jo; sameralali72@yahoo.com

[1] Faculty of Pharmacy, Isra University, P.O. Box 22, Amman 11622, Jordan

[2] Materials Synthesis and Characterization Laboratory, Institute of Advanced Technology (ITMA), University Putra Malaysia, Seri Kembangan, Malaysia

Published online: 01 August 2019

Different formulations with different independent variables should be optimized when developing pharmaceutical formulations. The challenges in optimizing of pharmaceutical formulation are due to the interaction between a lot of independent variables and individual pharmaceutical responses. Multiple regression analysis is a potent technique used for just one dependent and two or more independent (exploratory) variables [19, 20]. The variable whose value is to be predicted is known as the dependent variable or response (Y) and the ones whose known values are used for prediction are known as independent (exploratory) variables (of $X_1$, $X_2$, …, $X_k$) [21].

The aim of the present study is to prepare and optimize the formulation parameters of metronidazole-chitosan nanoparticles for pharmaceutical applications.

## Materials and methods

### Materials

The chemicals used in this study are metronidazole ($C_6H_9N_3O_3$ (99% purity), Sigma-Aldrich); low molecular weight chitosan (10–120 kDa, 90% deacetylation, Sigma-Aldrich) and sodium tripolyphosphate ((TPP), AZ chem., Sigma Aldrich). HPLC grade acetonitrile (99.8%, FW 41.05) was purchased from VWR (West Chester, PA). All other chemicals including acetic acid, calcium chloride, sodium phosphate dibasic, sodium phosphate monohydrate, and sodium chloride were purchased from Chem CO (England).

### Preparation of CSNPs and MET-CSNPs nanocomposites

Tripolyphosphate with negative charge has usually been used to prepare chitosan nanoparticles because of unique properties; such as nontoxic, multivalent and the ability to form gels through ionic interactions. The interaction can be controlled by the charge density of TPP and chitosan, which is controlled by pH of the solution [22]. CSNPs nanoparticles were prepared according to the procedure reported previously with some modifications [23]. CS (0.5, 1, 2%) was dissolved in 1% (*w/v*) acetic acid and sonicate until the solution became transparent. The addition of TPP solution with concentrations 0.5, 1, 2.5% were added to CS solution and controlled the pH at 4.5 using NaOH, with stirring at room temperature and stirring for 18 h. The product was centrifuged at 10000 rpm for 15 min and dried. The same procedure was repeated in order to form MET-CSNPs nanocomposites using different concentrations of MET (1%, 2%, and 4%). All the samples prepared are summarized in Table 1.

**Table 1** concentrations of CS, TPP and MET used to prepare MET-CSNPs nanocomposites

| In put variables concentrations (%) | | | | | | | |
|---|---|---|---|---|---|---|---|
| Samples | CS% | TPP% | Drug% | Samples | CS % | TPP% | Drug% |
| FS1 | 0.5 | 0.5 | 1 | FS15 | 1 | 1 | 4 |
| FS2 | 0.5 | 0.5 | 2 | FS16 | 1 | 2.5 | 1 |
| FS3 | 0.5 | 0.5 | 4 | FS17 | 1 | 2.5 | 2 |
| FS4 | 0.5 | 1 | 1 | FS18 | 1 | 2.5 | 4 |
| FS5 | 0.5 | 1 | 2 | FS19 | 2 | 0.5 | 1 |
| FS6 | 0.5 | 1 | 4 | FS20 | 2 | 0.5 | 2 |
| FS7 | 0.5 | 2.5 | 1 | FS21 | 2 | 0.5 | 4 |
| FS8 | 0.5 | 2.5 | 2 | FS22 | 2 | 1 | 1 |
| FS9 | 0.5 | 2.5 | 4 | FS23 | 2 | 1 | 2 |
| FS10 | 1 | 0.5 | 1 | FS24 | 2 | 1 | 4 |
| FS11 | 1 | 0.5 | 2 | FS25 | 2 | 2.5 | 1 |
| FS12 | 1 | 0.5 | 4 | FS26 | 2 | 2.5 | 2 |
| FS13 | 1 | 1 | 1 | FS27 | 2 | 2.5 | 4 |
| FS14 | 1 | 1 | 2 | | | | |

### Physico-chemical analysis and characterizations

#### Powder X-ray diffraction

The crystal phase identification of the prepared nanoparticles and nanocomposites samples was carried out using X-ray diffraction (XRD) at University Putra Malaysia-Malaysia. It is an advanced technique and it was widely used for the characterization of crystalline materials. The XRD technique was recorded in the range of 2–70° on a Shimadzu diffractometer, XRD-6000.

#### Infrared spectroscopy

FTIR is a technique used for identifying the functional groups and chemical bonds that are present in a molecule, interpreted from the observed infrared absorption spectrum. Each functional group has its own specific wave number/s and absorption characteristics, from which the functional group present in the sample can be inferred. Therefore, this technique can be used as supporting data, which complement other techniques to indicate that intercalation instead of adsorption has taken place.

For this purpose, Fourier transform infrared (FTIR) spectra of the materials were recorded over the range of 400–4000 $cm^{-1}$ on a Perkin Elmer (model Smart UAIR-two) with 4 $cm^{-1}$ resolutions.

#### The metronidazole loading efficiency

The ultra-centrifugation instrument was used to determine the loading efficiency (LE) of MET from prepared nanocomposites. The procedure was as follows: 2.0 ml of suspension was

centrifuged (Hettich Universal 30 RF) at 10000 rpm for 10 min in an ultra-filtration centrifuge. Finally, the free drug was measured by high performance liquid chromatography (HPLC, Shimadzu, Japan). The UV detection wavelength was 323 nm. Venusil C18 column (4.6 mm × 250 mm, 5 μm) was used to analyze the samples. The column temperature was kept at 25 °C. The mobile phase consisted of a mixture of acetonitrile/0.1% phosphoric acid (5:95, *v/v*) and the flow rate was 1.0 ml/min. The LE were calculated as follows [24]:

$$\%\text{Loading Efficiency (LE)} = \frac{T_p - T_f}{\text{mass of nanoparticles}} \times 100 \quad (1)$$

where $T_p$ is the total MET used to prepare the nanoparticles, and $T_f$ is the free MET in the supernatant.

### Particle size, and zeta potential of nanocomposites

Particle size and zeta potential of nanocomposites was analyzed through dynamic light scattering (DLS) with Zetasizer Nano S (Malvern, UK) at The Arab Pharmaceutical Manufacturing. The analysis was performed in triplicate at a temperature of 25 °C.

## Controlled release study of the metronidazole from the respective nanocomposites

In-vitro release of MET from nanocomposites is determined by primary method in 0.1 M HCl at pH 1.2, using a Perkin Elmer UV-Vis spectrophotometer with $\lambda_{max}$ of 323 nm. A suitable amount of each nanocomposites was added to 2 mL of the media. The cumulative amount of drug released into the solution was measured at preset time intervals at corresponding $\lambda_{max}$.

The percentage release of the MET into the release media was obtained by:

$$\%\text{Release} = \frac{\text{Concentration of MET at time t (ppm)}}{\text{Concentration corresponding to 100\%release of MET (ppm)}} \times 100 \quad (2)$$

The concentration which corresponds to 100% release was obtained by adding a known amount of nanocomposites in 2 mL HCl with using sonicate and heating the nanocomposites at 37 °C.

## Instrumentation

Powder X-ray diffraction (XRD) patterns were used to determine the crystal structure of the samples in the range of 2–70 degrees on an XRD-6000 diffractometer (Shimadzu, Tokyo, Japan) using $CuK_\alpha$ radiation (λ = 1.5406 Å) at 30 kV and 30 mA. Fourier transform infrared spectroscopy (FTIR) spectra of the materials were recorded over the range of 400–4000 $cm^{-1}$ on Perkin Elmer (model Smart UAIR-two). Thermogravimetric analysis was carried out using a Metter-Toledo 851e instrument (Switzerland) with a heating rate of 10 °C $min^{-1}$, in 150 μL alumina crucibles and in the range of 30 °C–900 °C. The zeta potential was measured at 25 °C by dynamic light scattering (DLS) using a Malvern Zetasizer Nano ZS (Malvern Instruments, Malvern, UK). UV-Vis spectra were measured to determine the release, using a Shimadzu UV-1601 spectrophotometer at Isra University.

# Results and discussion

## XRD for MET-CSNPs nanocomposites

XRD patterns of MET, CSNPs and MET-CSNPs are shown in Fig. 1(a–c), respectively. Standard MET powder showed a sharp peak at diffraction angles (2θ) of 12.1°, 13.8°, 24.5° and 29.3° suggesting that MET are highly crystalline in nature [25]. XRD spectra of CSNPs shows two peaks at 2θ = 12° and 23.7° (Fig. 1b) amorphous form due to cross-linked with TPP [26]. In case of MET-CSNPs, peaks of MET disappeared and MET became slightly amorphous once encapsulated into CSNPs, which showed absence of major peaks at 2θ = 12.1° and 24.5°. This result indicated that it is amorphous in nature.

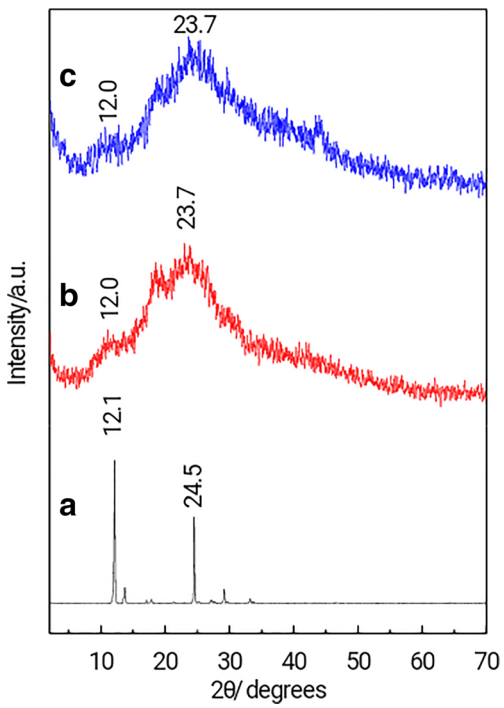


**Fig. 1** XRD diffraction spectra of MET (**a**), CSNPs (**b**) and MET-CSNPs (**c**)

## FTIR spectroscopic analysis of MET-CSNPs nanocomposites and chitosan–metronidazole interaction

Fig 2a–d demonstrates FTIR spectra of CS, CSNPs, MET and MET-CSNPs respectively. For CS, the absorption peak between 3086 and 3676 $cm^{-1}$ due to OH and $NH_2$ functional group [27]. The peak of C-H stretching appears at 2868 $cm^{-1}$. The absorption bands at 1650 $cm^{-1}$, 1574 $cm^{-1}$, and (2800–2900) $cm^{-1}$ are due to amide I band, N–H bending, and C–N stretching, respectively [28]. The peak of asymmetric stretch of C–O–C is found at around 1151 $cm^{-1}$. As seen from Fig. 2b, the peaks of amine I and N–H bending vibration shifted to 1534 $cm^{-1}$ (N–H stretching vibration of ammonium $NH_3^+$ group) and 1432 $cm^{-1}$, respectively, which may be due to strong ionic cross linking of chitosan with TPP [28]. The peak at 1156 $cm^{-1}$ due to C–O–C and P=O [29]. These results can be attributed to the linkage between phosphoric group of TPP and ammonium group of chitosan in nanoparticles

The peaks of MET in Fig. 2d indicate encapsulation of MET, such as the characteristic peaks of 2941 $cm^{-1}$ for C-H stretching, 1454 $cm^{-1}$ $CH_2$ bending, 1376 $cm^{-1}$ $CH_3$ bending and 1321 $cm^{-1}$ N=O asymmetric stretching [30].

Because of the cationic properties of chitosan nanoparticles, ion compounds can be formed by electrostatic interaction between amine group of chitosan and anionic nitro group of metronidazole (Fig. 3). This result can be confirmed by the bands centered at 1541 $cm^{-1}$ and 1379 $cm^{-1}$ of IR spectrum which assigned to the N–O stretching of nitro compound [31, 32].

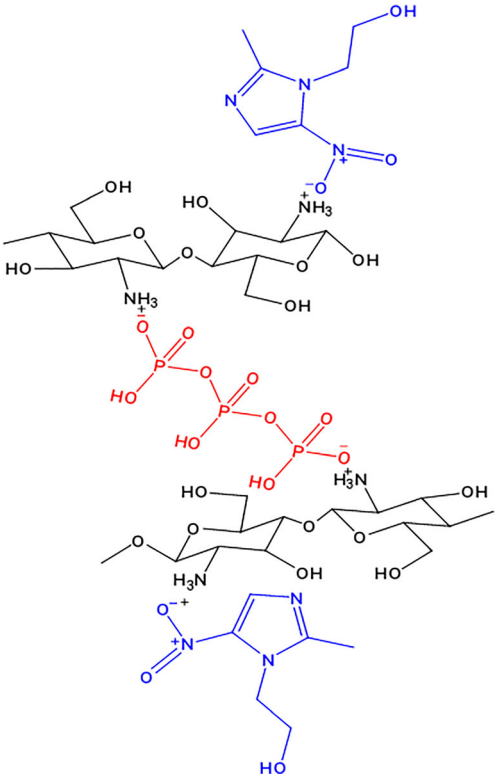

**Fig. 3** Interaction between CSNPs and MET

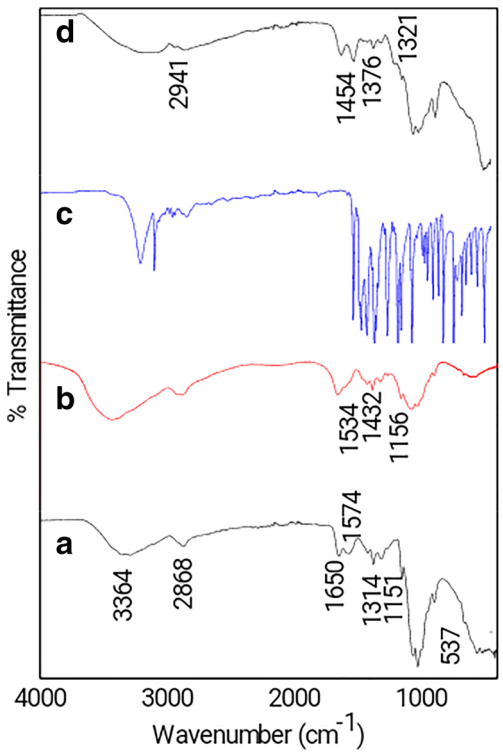


**Fig. 2** FTIR spectra of n-CS (**a**), CSNPs (**b**), MET (**c**) and MET-CSNPs (**d**)

## Thermogravimetric analysis of MET-CSNPs nanocomposites

The TGA curves of pure MET, CSNPs nanoparticles, and MET-CSNPs nanocomposites were shown in Fig. 4. For MET, only one main thermal events were clearly observed at 137–288 °C, which can be attributed to the decomposition and subtle combustion of MET, with a 99.1% weight loss [33].

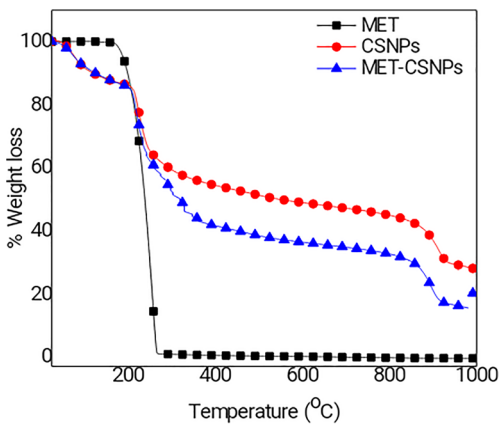


**Fig. 4** TGA curves are shown free MET, CSNPs and MET-CSNPs nanocomposites

The CSNPs nanoparticles show four main thermal stages. The first occurred between 25 and 178 °C, which can be to the moisture, with a 13.4% weight loss. This was followed by the second stage between 178 and 462 °C, which can be attributed to the decomposition of polymer [34, 35], corresponding to the strong peak at 276 °C and a 34.4% weight loss. Similarly, the third and the fourth stages appeared between 462–675 and 675–949 °C, with 5 and 18.4% weight loss [2].

The TGA of MET-CSNPs at Fig. 4 shows also four weight loss steps similar to CSNPs. But in case of MET-CSNPs, the second stage showed 42.2% weight loss comparing to 34.4% for CSNPs. The extra weight loss at this stage due to the incorporation of MET in the CSNPs.

## Scanning Electron microscopy (SEM)

The morphology of CSNPs was observed and the results were shown in (Fig. 5a) CSNPs revealed a very homogenous morphology and they are spherical in shape. SEM image of MET-CSNPs at Fig. 5b of the optimized formula showed also spherical particles, with uniform size distribution.

## Detection of multicollinearity in regression analysis

Multicollinearity occurs when independent variables in a regression model are correlated. This correlation will effect on the fit of the model. One method to evaluate multicollinearity is the variance inflation factor (VIF), which assesses how much the variance of an estimated regression coefficient increases if your predictors are correlated. If no factors are correlated, the VIFs will all be 1 value.

Based on the absence of Multicollinearity from the readings in this work (Table 2), the data will be analyzed statistically using Multivariate regression model.

## Multiple linear regression analysis using stepwise method

There are different selection methods for linear regression modeling in order to state how independent variables are used into the analysis. Simultaneous, stepwise, forward and backward elimination are examples of these methods. By using these methods, a variety of regression models from the same set of variables could be constructed. All variables must pass the tolerance criterion to be entered in the equation, regardless of the entry method specified. A variable is not entered if it would cause the tolerance of another variable already in the model to drop below the tolerance criterion [36]. In a model fitting the variables to be inserted and removed from the model and various goodness-of-fit statistics are displayed such as $R^2$, R squared change, standard error of the estimate, and an analysis-of-variance table.

Our data was analyzed using Minitab software using stepwise multiple linear regression models. Stepwise regression method was removing the weakest correlated variable. At the end it will leave the variables that explain the distribution best.

$$Y = \beta 0 + \beta 1\ X1 + \ldots + \beta \rho X \rho + \sigma(\Upsilon)$$

Y is the dependent variable (LE, particle size and zeta potential), $\beta 0$ = intercept, $\beta 1 \ldots \beta \rho$ = regression coefficients of independent variable CS, TPP and MET concentration.

Table 2 shows the statistical data after using Minitab software and remove the non-significant variable and re-fit the model excluding the data. The excluded variable for LE model was TPP, whereas for Potential model the CS and MET were the excluded variables.

R-squared is a statistical measure of how close the data are to the fitted regression line. At Table 4 the R-squared value for

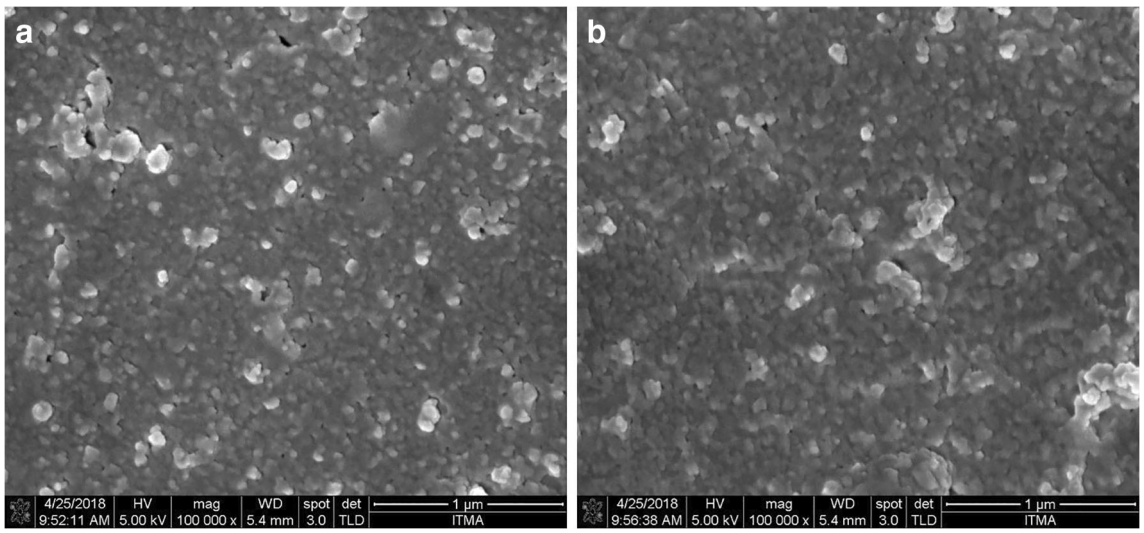


**Fig. 5** SEM images of CSNPs nanoparticles (**a**) and MET-CSNPs nanocomposites (**b**)

**Table 2** Summary Statistics of MET-CSNPs nanocomposites

| | LE | | Size | | | Potential |
|---|---|---|---|---|---|---|
| | Fitting model | | Fitting model | | | Fitting model |
| Adj SS | 13698 | | 743080 | | | 589.5 |
| Adj MS | 6849.1 | | 247693 | | | 589.5 |
| F | 26.64 | | 20.02 | | | 42.00 |
| P | 0.000 | | 0.000 | | | 0.000 |
| S | 16.0338 | | 111.229 | | | 3.74652 |
| R-sq | 71.73% | | 75.97% | | | 66.67% |
| R-sq (adj) | 69.04% | | 72.17% | | | 65.08% |
| R-sq (Pred) | 63.26% | | 63.19% | | | 60.20% |
| Coef | 55.72 | | 282.7 | | | 40.25 |
| SE-Coef | 8.84 | | 81.5 | | | 1.50 |
| T-Value | 6.30 | | 3.47 | | | 26.85 |
| | **CS** | **MET** | **CS** | **TPP** | **MET** | **TPP** |
| AdjSS | 10265 | 4295 | 162553 | 217598 | 330532 | 589.5 |
| AdjMS | 10264.5 | 4295.2 | 162553 | 217598 | 330532 | 589.5 |
| F value | 39.93 | 16.71 | 13.14 | 17.59 | 26.72 | 42.00 |
| *P* value | 0.000 | 0.001 | 0.002 | 0.000 | 0.000 | 0.000 |
| T value | −6.32 | 4.09 | 3.62 | −4.19 | 5.17 | 26.85 |
| VIF | 1.00 | 1.00 | 1.03 | 1.03 | 1.06 | 1.00 |
| | LE= | | Size= | | | Potential= |
| | 55.72 | | 282.7 | | | 40.25 |
| | - 32.54 CS + 10.75 MET | | + 139.5 CS | | | – 5.779 TPP |
| | | | – 122.6 TPP | | | |
| | | | + 103.6 MET | | | |

LE, size and potential model was 71.73%, 75.97% and 66.67%, respectively. Furthermore, these three models have statistically significant predictors; indicate the models can still draw important conclusions about how changes in the predictor values are associated with changes in the response value.

The Table 2 also shows the variance inflation factor (VIF) for selected predictor at models was less than 5, indicated the absence of the multicollinearity.

## Effect of CS, MET and TPP concentrations on loading efficiency, particles size and zeta potential of MET-CSNPs nanocomposites

The effect of CS, TPP and MET concentrations on the loading efficiency, zeta size and zeta potential were examined as shown in Table 3.

### CS concentration

The effect of chitosan concentration on loaded efficiency was also examined in this study and it was found that the loading efficiency increased with the increased CS concentration from 0.5 to 1.0% at 0.5 and 2.5% of TPP. This can be explained by the increasing concentration of the chitosan, leading to increased physical entrapment of MET.

However, in some samples prepared, the loading efficiency decreased at high chitosan concentration. This result can be explained through the aggregation behavior; the particle size increased with increase in polymer concentration, which leads to the aggregation of the product. (Section 3–10).

The effect of different chitosan concentrations on the size of nanoparticles is also shown in Table 3. Our results showed that by increasing the chitosan concentration from 0.5 to 2.0% at a constant TPP concentration and MET, the size of nanoparticles increased from 190 nm to 800 nm [37]. The PDI value of nanoparticles with chitosan concentration of 2% and some of 1% was not within the acceptable range, as shown by the formation of aggregates with large diameters. The PDI value of particles was more favorable at chitosan concentration of 0.5% than 2%, indicating mid-range polydispersity. The effect of CS concentration can be explained by the fact that adding more amounts of the chitosan starting material to the vessel reaction increases the probability of interaction of chitosan polymers to form larger particles. From Table 2 at 4% and 2% MET, increasing the chitosan concentration lead to decrease in the size from 466 nm to 293 nm and from 300 nm to 280 nm, respectively.

**Table 3** data collected from different formulations prepared at different variables changes

| Samples | Outcome Variables | | | | | | |
|---|---|---|---|---|---|---|---|
| | %LE | Size (nm) | Potential (mV) | Samples | %LE | Size (nm) | Potential (mV) |
| FS1 | 52.1 | 350.6 | 33.7 | FS15 | 9.1 | 806 | 32.1 |
| FS2 | 79.7 | 403.1 | 22.5 | FS16 | 45.1 | 228.1 | 30.8 |
| FS3 | 88.4 | 778.4 | 40 | FS17 | 51.4 | 270.8 | 25.7 |
| FS4 | 26.1 | 357.3 | 40 | FS18 | 87.8 | 224.5 | 25.9 |
| FS5 | 72.2 | 438.4 | 40.7 | FS19 | 10.5 | 740.3 | 38.2 |
| FS6 | 75.3 | 465.7 | 40.1 | FS20 | 6.2 | 800 | 60.7 |
| FS7 | 33.5 | 228.1 | 20.4 | FS21 | 7.6 | 830 | 43.2 |
| FS8 | 46.1 | 881.6 | 27.1 | FS22 | 7.5 | 357.3 | 44.3 |
| FS9 | 71.8 | 574.9 | 28.2 | FS23 | 10.5 | 806 | 35.4 |
| FS10 | 56.1 | 529.7 | 32 | FS24 | 17.1 | 292.8 | 32.2 |
| FS11 | 84.6 | 442.8 | 31.7 | FS25 | 64.2 | 409.9 | 23.1 |
| FS12 | 91.5 | 806 | 37.5 | FS26 | 23.1 | 279.9 | 25 |
| FS13 | 21.5 | 365.9 | 42.4 | FS27 | 39.8 | 242.5 | 23.7 |
| FS14 | 23.6 | 566.7 | 31.1 | | | | |

In general, the stability of nanoparticles depends on the charge, where the ideal for physical stability of any suspension was > +30 mV and < -30 mV [29]. Zeta potential studies of the MET-CSNPs nanocomposites showed the values ranging from 20.4 ± 3.4 to 60.7 ± 4.6 mV. In general, it was noted that zeta potential of the nanocomposites increased as the chitosan concentration increased at 0.5% TPP; this can be attributed to ammonium ($NH_4^+$). The chitosan concentrations at Table 3 did not have a significant effect on the zeta potential.

## MET concentrations

In the present study the effect of MET concentration (1, 2, and 4%) has assessed loading efficiency. MET loading efficiencies increased with MET concentration at 0.5 and 1.0% of CS. These findings were consistent with previous studies demonstrating that drug loading onto chitosan particles was directly related to the concentration of the drug [38]. Our data indicate that elevating the MET concentration from 1 to 4% leads to an increase of loading efficiency from 26.1% to 72.2% at 0.5% CS and 1% TPP condition.

Table 3 shows the effect of MET concentrations on the particle size. As depicted in the table, it was observed that decreasing the amount of MET resulted in better particle size. From the table, concentration at 1% mg of MET at 0.5% CS and 0.5% TPP showed better size compared to the same conditions at 4% [39]. At samples prepared (2.0% CS and 2.5% TPP), increasing the concentration of MET, lead to decrease of the particle size.

## TPP concentrations

The effects of chitosan-to-TPP mass ratio on the loading efficiency of nanoparticles were studied at the different mass ratio at a fixed CS concentration of 0.5 and 2.0%, and the results are presented in Table 4. The loading efficiency of nanoparticles decreased with the decrease in weight ratio of CS/TPP. A possible explanation may be that a more compact solid-matrix structure resulted due to the increased mass ratio for CS/TPP, which leads to the increasing amount of formed nanoparticles, resulting in the increase in loading efficiency in nanoparticles [39]. In addition, as the ratio of chitosan to TPP increases, the surface charge in the nanoparticles will also increase. This may have resulted in higher loading of MET due to increased ionic interaction between MET and chitosan [40].

The effect of CS/TPP mass ratio on the particle size was studied in this work at a fixed CS concentration of 0.5 and 2.0%. The particle size decreased with the decreasing of CS-TPP mass ratio from 1:1 to 0.5:1 and 4:1 to 2:1, as shown in

**Table 4** the effects of chitosan to TPP mass ratio on the loading efficiency and size of MET-CSNPs nanocomposites

| CS/TPP mass ratio | CS% | MET% | %LE | Size (nm) |
|---|---|---|---|---|
| 1:1 | 0.5 | 1 | 50.7 ± 0.43 | 350.6 |
| 0.5:1 | | | 27.2 ± 0.92 | 331.2 |
| 1:1 | 0.5 | 2 | 80.7 ± 0.49 | 403.1 |
| 0.5:1 | | | 70.8 ± 0.35 | 438.3 |
| 1:1 | 0.5 | 4 | 87.7 ± 0.49 | 677.4 |
| 0.5:1 | | | 70.5 ± 0.10 | 465.7 |
| 4:1 | 2.0 | 1 | 7.8 ± 1.77 | 740.3 |
| 2:1 | | | 8.3 ± 0.42 | 357.3 |
| 4:1 | 2.0 | 2 | 6.3 ± 0.35 | 800 |
| 2:1 | | | 7.6 ± 0.21 | 325.1 |
| 4:1 | 2.0 | 4 | 7.4 ± 0.49 | 830 |
| 2:1 | | | 16.6 ± 0.24 | 292.9 |

Table 4. According to the literature, CS has the ability to form inter- and intramolecular crosslinking between the amino groups and the phosphate groups. This effect leads to penetration of the drug molecule in chitosan network, activating hydroxyl sites and establishing physical–chemical electrostatic interactions and hydrogen bonds in the new system.

In addition, the lower zeta potential with increasing TPP amounts at chitosan concentration 1% and 2% might be caused by an increased masking of free positively charged amino groups of chitosan [39]. In all samples prepared in Table 4, MET concentration did not have a significant effect on zeta potential.

## Statistical data analysis for LE, size model and zeta potential

### Residuals versus observation order

Fig 6a, b and c shows the residuals versus observation order plot for dependent variables LE, size and potential, respectively, to attest the hypothesis that the residuals are independent from one another. From the figure, independent residuals show no fixed trends when displayed in time order, thus, not independent. This is because, the residuals on the plot fall randomly around the center line.

### Residuals versus fitted value

In general, the residuals figure versus fits plot was used to verify the assumption that the residuals are randomly distributed and have constant variance. At Fig. 7a, b and c, all points fall randomly on both sides of 0, with no recognizable patterns in the points, indicating randomly distribution for LE, size and zeta potential.

### Normal probability plot

The normal probability plot is a graphical method for evaluating whether a data set is nearly normally distributed or not [41]. The data are plotted against a theoretical normal distribution in such a way that the points should form a near straight line. Departures from this straight line indicate departures from normality. The normal probability plot is a special case of the probability. We cover the normal probability plot separately due to its importance in many applications. The points at Fig. 8a, b and c for LE, size and zeta potential have normal probability plot of 40 normal random numbers form a nearly linear pattern, which indicates that the normal distribution is a good model for this data set.

### Contour plot and surface plot of LE and size against selected independent variables

Contour plots are diagrammatic representation of the values of the responses that help in explaining the relationship between independent and dependent variables. Fig 9a-1 shows the contour plot of LE against the CS and MET. The highest values of LE are in the upper left corner of the plot, which corresponds with high values of MET and low value of CS. Similarly, the surface is maximum (Fig. 9a-2).

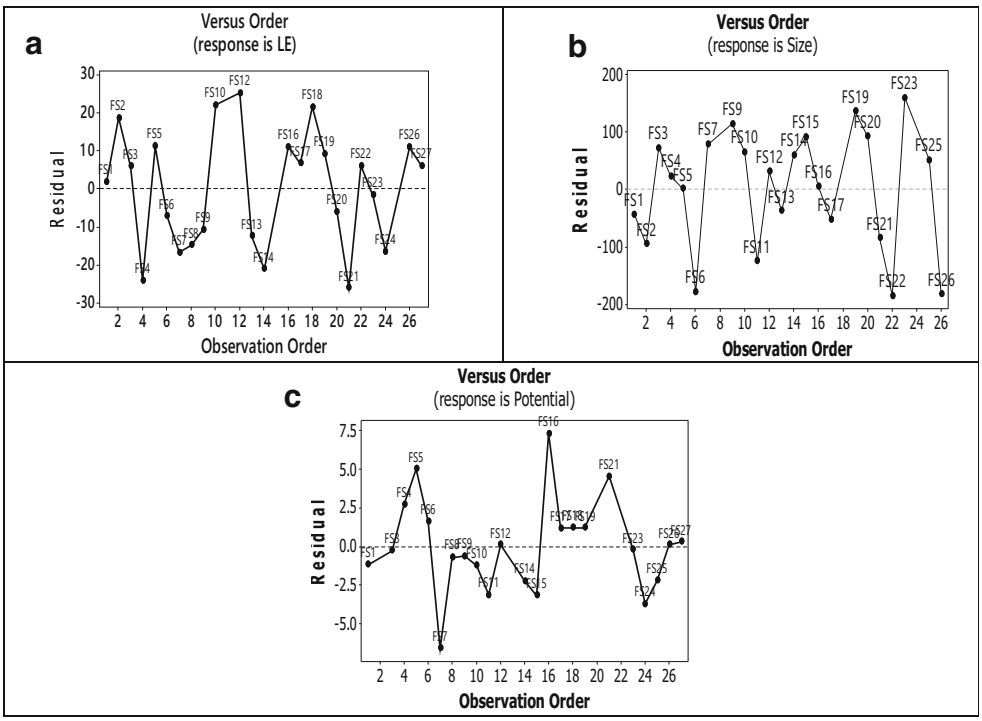


**Fig. 6** Residuals versus observation order for LE (**a**), size (**b**) and potential (**c**)

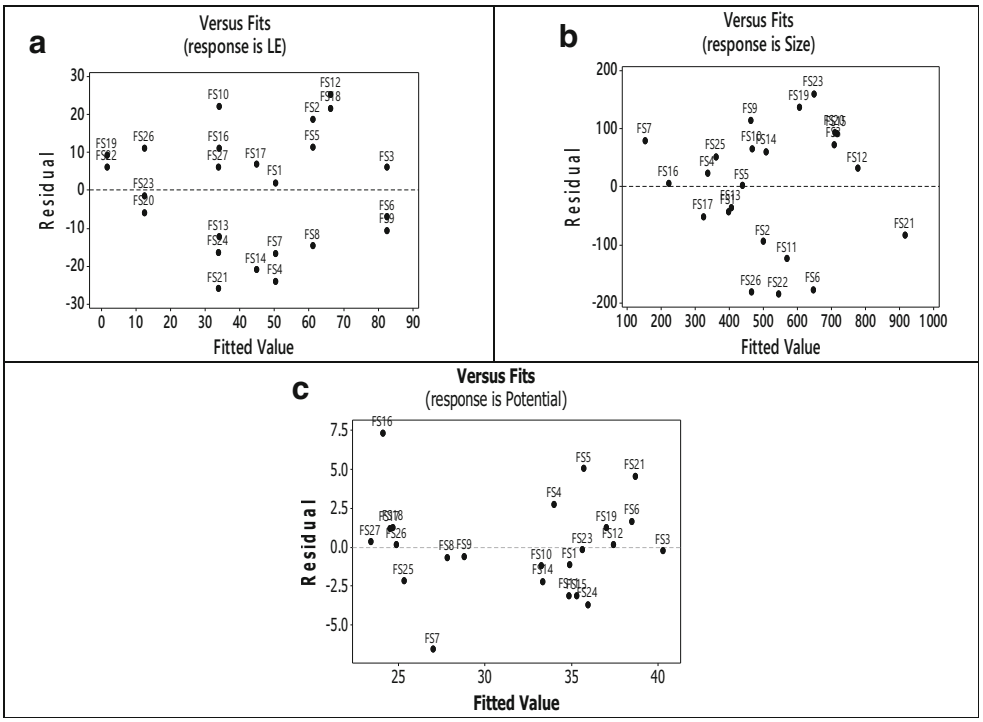


**Fig. 7** Residuals versus fitted value for LE (**a**), size (**b**) and potential (**c**)

Two-dimensional contour plots were established between CS and TPP, CS and MET, and TPP and MET for size at Fig. 10(a–c), respectively. The plots showed that size was greatly dependent on CS and TPP concentrations (Fig. 10a-1). When CS variables at their minimum levels and the TPP at maximum level, size was found to be minimum, and the surface is minimum (Fig. 10a-2). However, the contour of CS vs. MET concentration (Fig. 10b-1) showed that both these variables were at their minimum levels, size was also found to be minimum, and the surface is minimum (Fig. 10b-2). It was concluded from the contours that high concentration of TPP but low concentration of MET and CS was required for lowest size in preparation of MET-CSNPs nanocomposites (Fig. 10c-1), the surface is minimum (Fig. 10c-2).

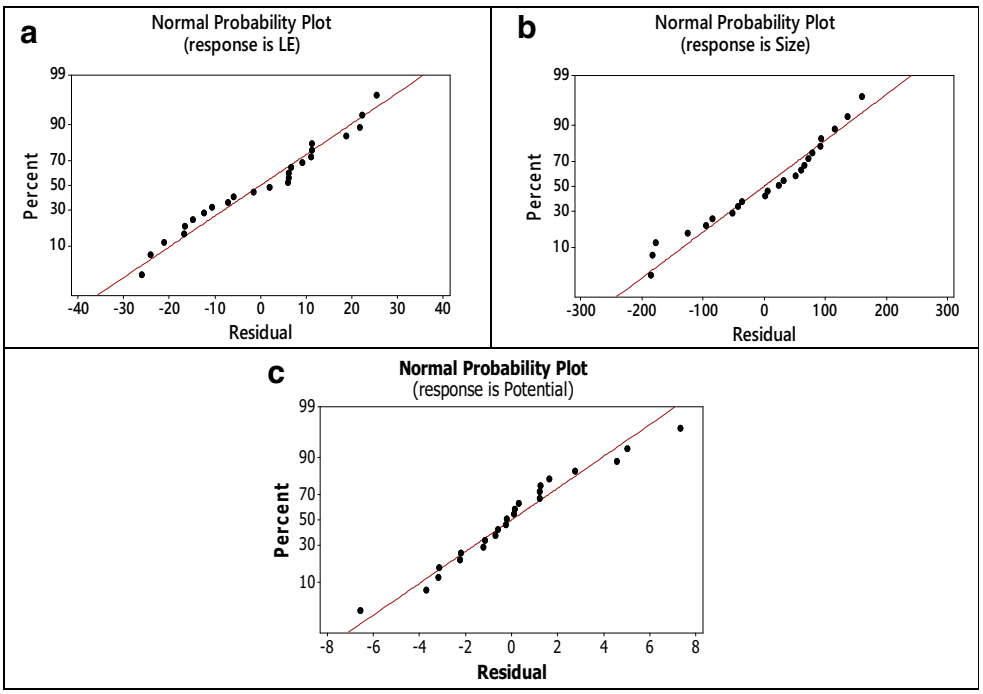


**Fig. 8** Normal probability plots for LE (**a**), size (**b**) and potential (**c**)

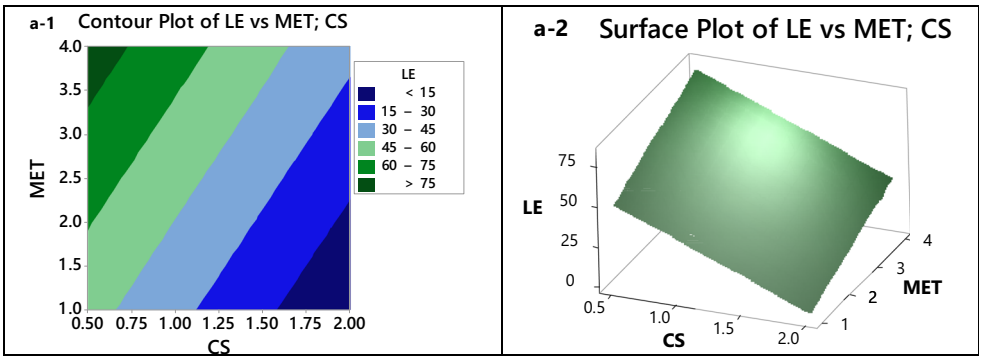


**Fig. 9** Contour plots and surface plot of LE against selected independent variables

## Optimization of LE and size formulations

According to our criteria for highest LE (81.8%), the optimized CS and MET concentrations under canonical analysis were selected at 0.5192 and 4 mg, respectively (Fig. 11a). In addition, the minimum size (149 nm) optimized by using following concentrations; CS 0.5 mg, TPP 2.5 mg and MET 1 mg (Fig. 11b).

## Poly dispersion index and CS-MET nanoparticles aggregation

In the field of Polymeric Materials, poly dispersion index (PDI) is defined as the average weight (Mw) divided by number average molecular weight (Mn) (eq. 3). Its indicates ~~on~~ the average uniformity of a particle solution, where larger PDI values relate to a larger size distribution in the particle sample.

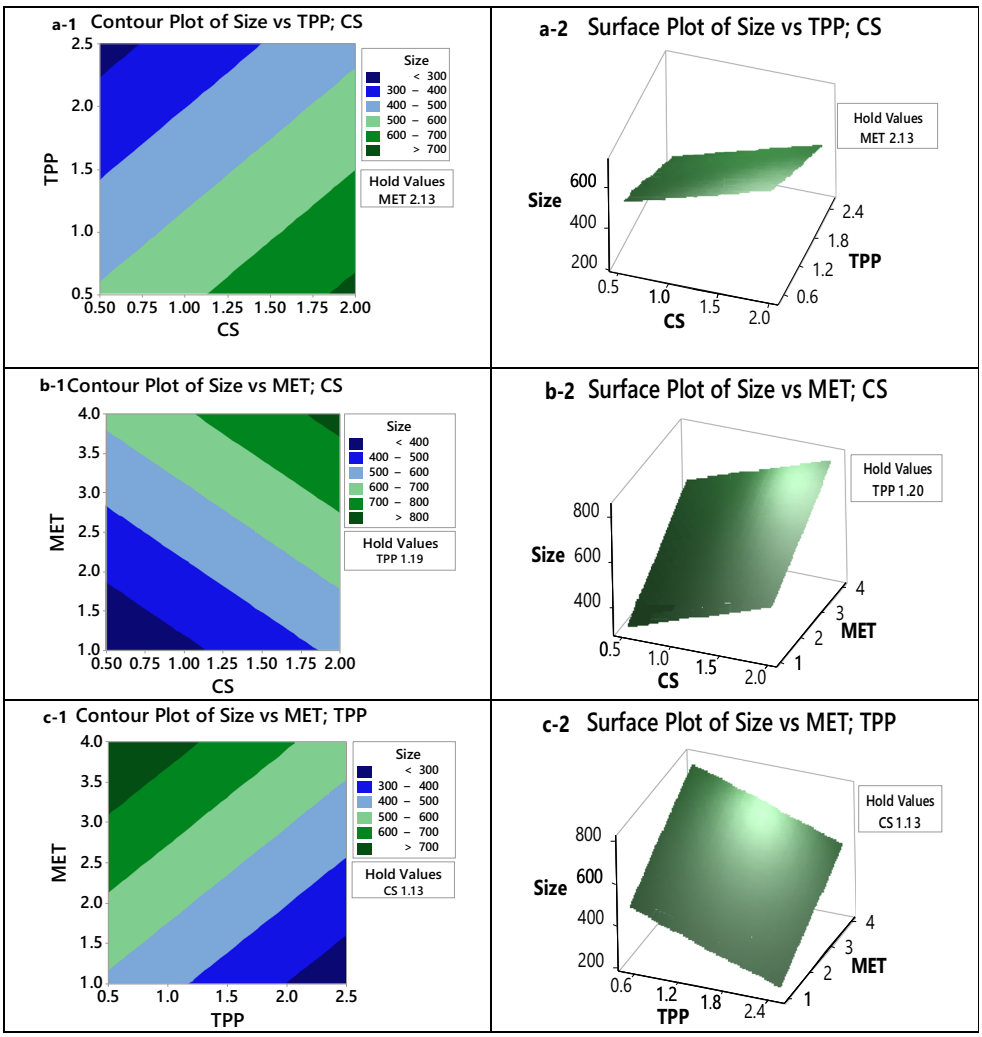


**Fig. 10** Contour plots and surface plot of size against independent variables

It also indicates nanoparticles aggregation for particle surface modifications throughout the particle sample. A sample is considered monodisperse when the PDI value is less than 0.1 [42]. PDI values between 0.05 and 0.7 indicate that the sample has a broad particle size distribution [43].

$$\mathrm{PdI} = \left(\frac{M_w}{M_n}\right) \tag{3}$$

Contours plots which are graphic representation make relationships between three numeric variables in two dimensions. Two variables are for X and Y axes, and a third variable Z is for contour levels. The contour levels are plotted as curves; the area between curves can be color-coded to indicate interpolated values. Figure 12a-1 shows the contour plot of PDI against the CS and TPP concentrations. The highest values of PDI are in the higher right and lower left of the plot, which correspond to high values of CS and TPP (higher right) and low values of CS and TPP (higher right), and the surface is maximum (Fig. 12a-2).

The Fig. 12b-1 showed that PDI was dependent on CS and MET concentrations. The highest values of PDI are in the lower right and higher left of the plot, which correspond to high values of CS and low value of MET (lower right) and low values of CS and high value of MET (higher left), and the surface is maximum (Fig. 12b-2).

When TPP and MET variables are at their minimum and maximum levels, the PDI shows highest values (Fig. 12c-1), PDI was found to be maximum surface (Fig. 12c-2).

## Release study of MET from MET-CSNPs nanocomposites

MET release from the nanocomposites seen in Fig. 13 can occur in two parts: "burst release" and "extended release". The initial burst phase during the first hour is caused by MET adsorbed on the surface of the CSNPs, while the extended release of the MET after 1 h is caused by the slow diffusion of MET from the polymer matrix [44, 45]. From Fig. 13, it was very clear that about 15, 19, 15, 62% of the a, b, c and d nanocomposites, respectively, were released after 1 h. The final point release for samples a, b, c, and d detected are 62%, 92%, 98% and 100% at times 23, 24, 16, and 7 h, respectively.

## Release kinetics of MET from the MET-CSNPs nanocomposites

The data of the cumulative release of the MET from nanocomposites were fitted to five kinetic models which generally are described as follows:

1. The linear form of first-order kinetic model as Eq. (4) [46]

$$\ln\left(q_e - q_t\right) = \ln q_e - k_1 t \tag{4}$$

in which $q_e$ and $q_t$ are the quantity released at equilibrium and the quantity released at any time (t), respectively, and $k_1$ is the rate constant of the pseudo-first-order release kinetics.

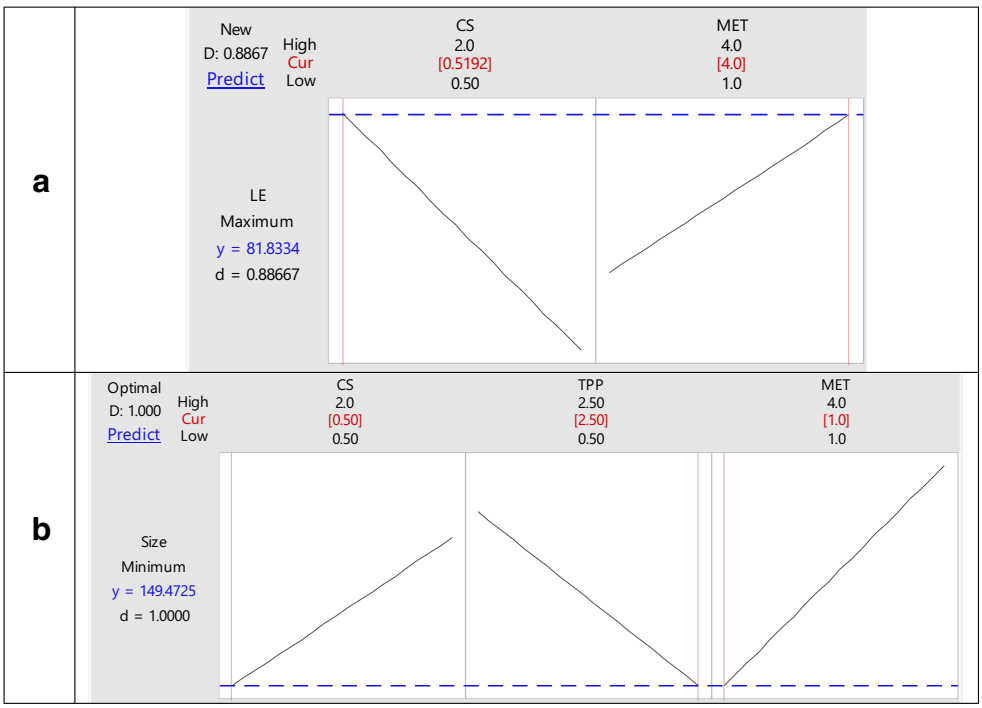


**Fig. 11** the optimized concentrations of the selected independent variables against LE and size responses

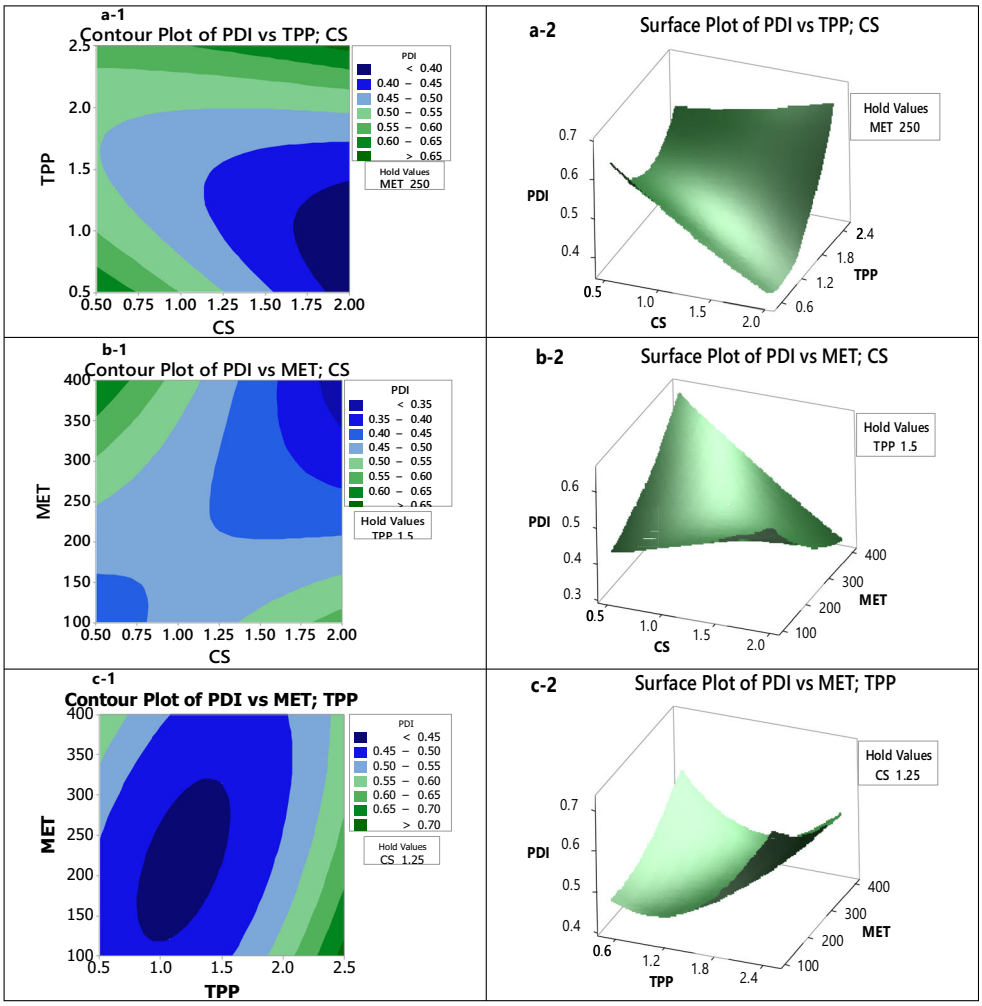


**Fig. 12** Contour plots and surface plot of PDI against CS, TPP and MET variables

2. The linear form of second-order kinetic equation may be represented in Eq. (5) [47]

$$t/q_t = 1/k_2 q_e^{\,2} + t/q_e \tag{5}$$

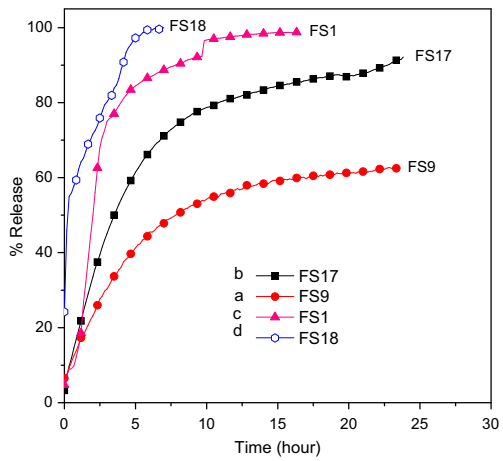


**Fig. 13** In vitro release behaviors of MET from MET-CSNPs nanocomposites in the 0.1 N HCl

Where, $k_2$ is the rate constant of the pseudo-second-order release kinetics.

3. The Higuchi model describes the increased release of the drug from the nanocomposites with increasing the square root of time [48]

$$q_t = K_H\sqrt{t} \tag{6}$$

in which $k_H$ is the Higuchi rate constant.

4. The Hixson-Crowell model gives the relationship between the cube root of the percentage of drug remaining in the nanocomposites as a function of time [48]

$$\sqrt[3]{M_o} - \sqrt[3]{q_t} = Kt \tag{7}$$

in which $M_o$ is the initial quantity of drug in the nanocomposites and $q_t$ is the quantity released at time t.

5. The Korsmeyer-Peppas model gives the relationship between the log of percentage of drug released and the log of time [48]

**Table 5** The correlation coefficients ($R^2$) obtained by fitting the MET release data from MET-CSNPs nanocomposites in 0.1 N HCl

| Samples | $R^2$ | | | |
|---|---|---|---|---|
| | First order | Second order | Hixson-Crowell model | Korsmeyer-Peppas model |
| A=FS9 | 0.908 | 0.995 | 0.745 | 0.921 |
| B=FS17 | 0.944 | 0.996 | 0.844 | 0.838 |
| C=FS1 | 0.969 | 0.948 | 0.894 | 0.780 |
| D = FS18 | 0.896 | 0.984 | 0.970 | 0.700 |

$$\frac{q_t}{q_\infty} = Kt^n \quad (8)$$

in which $q_\infty$ is the release at infinite time.

The MET release from nanocomposites was discussed by first order kinetics, second order kinetics, Hixson-Crowell model, and Korsmeyer-Peppas model. From Table 5, it can be found that the A, B and D nanocomposites were fitted into second-order kinetics model with $R^2$ value 0.995, 0.996, 0.984, respectively; whereas, the C nanocomposites were fitted into first-order kinetics model with $R^2$ 0.969 value.

## Conclusion

The present work established the use of multiple regression analysis as data analysis approach to understand the effect of various formulation variables in the prediction of %LE and particle size of MET-CSNPs nanocomposites. MET-CSNPs exhibited extended release and followed first and second release kinetics. Therefore, by using these formulations, the oral delivery of metronidazole drugs for the treatment of patients is now possible.

**Acknowledgements** This study was also supported by Hikma pharmaceuticals Research and development Department. Special thanks to "Ahmad Abu Sharar, R&D Project leader" for his insights and expertise that greatly assisted the researcher in Hikma Pharmaceuticals Co.

**Funding** The author would like to thank the Faculty of Pharmacy at Isra University, and University Putra Malaysia under grand number (9443100 NANOMITE) provided funding for this research.

### Compliance with ethical standards

**Conflicting interests** The authors report no conflicts of interest in this work.

## References

1. Baghdan E, Pinnapireddy SR, Strehlow B, Engelhardt KH, Schäfer J, Bakowsky U (2018) Lipid coated chitosan-DNA nanoparticles for enhanced gene delivery. Int J Pharm 535(1):473–479
2. Hussein-Al-Ali SH et al (2018) Preparation of chitosan nanoparticles as a drug delivery system for perindopril erbumine. Polym Compos 39(2):544–552
3. Porras-Gómez M, Matamoros J, and Vega-Baudrit J 2013 Chitosan nanoparticles for biomedical applications
4. Kaolaor A, Phunpee S, Ruktanonchai UR, Suwantong O (2019) Effects of β-cyclodextrin complexation of curcumin and quaternization of chitosan on the properties of the blend films for use as wound dressings. J Polym Res 26(2):43
5. Pandey AR, Singh US, Momin M, Bhavsar C (2017) Chitosan: application in tissue engineering and skin grafting. J Polym Res 24(8):125
6. Key J, Park K (2017) Multicomponent, tumor-homing chitosan nanoparticles for Cancer imaging and therapy. Int J Mol Sci 18(3)
7. Patil AS, Gadad AP, Hiremath RD, Joshi SD (2018) Biocompatible tumor micro-environment responsive CS-g-PNIPAAm co-polymeric nanoparticles for targeted Oxaliplatin delivery. J Polym Res 25(3):77
8. Choi SJ, Choy JH (2011) Layered double hydroxide nanoparticles as target-specific delivery carriers: uptake mechanism and toxicity. Nanomedicine 6(5):803–814
9. Shi W, Wei M, Jin L, Li C (2007) Calcined layered double hydroxides as a. J Mol Catal B Enzym 47(1–2):58–65
10. Williams GR, O'Hare D (2006) Towards understanding, control and application of layered double hydroxide chemistry. J Mater Chem 16(30):3065–3074
11. Jayakumar R, Menon D, Manzoor K, Nair SV, Tamura H (2010) Biomedical applications of chitin and chitosan based nanomaterials—a short review. Carbohydr Polym 82(2):227–232
12. Pillai C, Paul W, Sharma CP (2009) Chitin and chitosan polymers: chemistry, solubility and fiber formation. Prog Polym Sci 34(7): 641–678
13. Muzzarelli RAA (1973) Natural chelating polymers; alginic acid, chitin, and chitosan. 1st ed. international series of monographs in analytical chemistry, v 55, Oxford, New York: Pergamon Press. xii, p 254
14. Zikakis JP (1984) Chitin, chitosan, and related enzymes. Orlando: Academic Press. xxiv, 423 p
15. Kumar MNR (2000) A review of chitin and chitosan applications. React Funct Polym 46(1):1–27
16. Rowe RC (2006) Handbook of pharmaceutical excipients / edited by Raymond C. Rowe, Paul J. Sheskey, Siân C. Owen. 5th ed., London; Greyslake, IL Washington, DC: Pharmaceutical Press; American Pharmacists Association. xxi, 918 p
17. Xia W, Liu P, Zhang J, Chen J (2011) Biological activities of chitosan and chitooligosaccharides. Food Hydrocoll 25(2):170–179
18. Bhatia S (2016) Natural polymer drug delivery systems: nanoparticles, plants, and algae. Springer
19. Lee C-H, Nalluri LP, Popuri SR (2018) Optimization studies for encapsulation and controlled release of curcumin drug using Zn+2 cross-linked alginate and carboxy methylcellulose blend. J Polym Res 26(1):13
20. Singireddy A, Pedireddi SR, Subramanian S (2019) Optimization of reaction parameters for synthesis of Cyclodextrin nanosponges in controlled nanoscopic size dimensions. J Polym Res 26(4):93
21. Alexopoulos EC (2010) Introduction to multivariate regression analysis. Hippokratia 14(Suppl 1):23–28

22. Zhao L-M, Shi LE, Zhang ZL, Chen JM, Shi DD, Yang J, Tang ZX (2011) Preparation and application of chitosan nanoparticles and nanofibers. Braz J Chem Eng 28(3):353–362
23. Pant A, Negi JS (2018) Novel controlled ionic gelation strategy for chitosan nanoparticles preparation using TPP-β-CD inclusion complex. Eur J Pharm Sci 112:180–185
24. Omid NJ, Babanejad N, Amini H, Amini M, Rafiee Tehrani M, Dorkoosh F (2014) Preparation and characterization of novel derivatives of chitosan and trimethyl chitosan conjugated with dipeptides and vitamin B12 as candidates for oral delivery of insulin. J Polym Res 21(8):510
25. Caira MR, Nassimbeni LR, Van Oudtshoorn B (1993) X-ray structural characterization of anhydrous metronidazole benzoate and metronidazole benzoate monohydrate. J Pharm Sci 82(10):1006–1009
26. Nagarwal RC, Nath Singh P, Kant S, Maiti P, Pandit JK (2011) Chitosan nanoparticles of 5-fluorouracil for ophthalmic delivery: characterization, in-vitro and in-vivo study. Chem Pharm Bull 59(2):272–278
27. Liu C-G, Desai KGH, Chen XG, Park HJ (2005) Preparation and characterization of nanoparticles containing trypsin based on hydrophobically modified chitosan. J Agric Food Chem 53(5):1728–1733
28. Aydin R, Pulat M (2012) 5-fluorouracil encapsulated chitosan nanoparticles for pH-stimulated drug delivery: evaluation of controlled release kinetics. J Nanomater 2012:42
29. Nallamuthu I, Devi A, Khanum F (2015) Chlorogenic acid loaded chitosan nanoparticles with sustained release property, retained antioxidant activity and enhanced bioavailability. Asian J Pharm Sci 10(3):203–211
30. Trivedi, M.K., et al. (2015) Spectroscopic characterization of biofield treated metronidazole and tinidazole
31. Martins AF, Pereira AGB, Fajardo AR, Rubira AF, Muniz EC (2011) Characterization of polyelectrolytes complexes based on N, N, N-trimethyl chitosan/heparin prepared at different pH conditions. Carbohydr Polym 86(3):1266–1272
32. Anand M, Sathyapriya P, Maruthupandy M, Hameedha Beevi A (2018) Synthesis of chitosan nanoparticles by TPP and their potential mosquito larvicidal application. Front Lab Med 2(2):72–78
33. de Souza N et al (2003) Thermal stability of metronidazole drug and tablets. J Therm Anal Calorim 72(2):535–538
34. Mathew S, Brahmakumar M, Abraham TE (2006) Microstructural imaging and characterization of the mechanical, chemical, thermal, and swelling properties of starch–chitosan blend films. Biopolymers 82(2):176–187
35. Sarmento B, Ribeiro A, Veiga F, Ferreira D (2006) Development and characterization of new insulin containing polysaccharide nanoparticles. Colloids Surf B: Biointerfaces 53(2):193–202
36. SPSS S (2006) 15.0 command syntax reference. SPSS Inc
37. Ponnuraj R et al (2015) Formulation and characterization of rosuvastatin calcium nanoparticles. Indo Am J Pharm Res 5:767–779
38. Zhang H-l et al (2010) Preparation and characterization of water-soluble chitosan nanoparticles as protein delivery system. J Nanomater 2010:1
39. Hou D, Gui R, Hu S, Huang Y, Feng Z, Ping Q (2015) Preparation and characterization of novel drug-inserted-montmorillonite chitosan carriers for ocular drug delivery. Adv Nanoparticles 4(03):70–84
40. Fee M (2006) Evaluation of chitosan stability in aqueous systems. University of Nottingham
41. Tukey P (1983) Graphical methods for data analysis. Wadsworth, Belmont
42. Hughes JM, Budd PM, Tiede K, Lewis J (2015) Polymerized high internal phase emulsion monoliths for the chromatographic separation of engineered nanoparticles. J Appl Polym Sci 132(1)
43. Danaei M, Dehghankhold M, Ataei S, Hasanzadeh Davarani F, Javanmard R, Dokhani A, Khorasani S, Mozafari M (2018) Impact of particle size and polydispersity index on the clinical applications of lipidic nanocarrier systems. Pharmaceutics 10(2):57
44. Fan Y-L, Fan BY, Li Q, di HX, Meng XY, Ling N (2014) Preparation of 5-fluorouracil-loaded nanoparticles and study of interaction with gastric cancer cells. Asian Pac J Cancer Prev 15(18):7611–7615
45. Che Y, Li D, Liu Y, Yue Z, Zhao J, Ma Q, Zhang Q, Tan Y, Yue Q, Meng F (2018) Design and fabrication of a triple-responsive chitosan-based hydrogel with excellent mechanical properties for controlled drug delivery. J Polym Res 25(8):169
46. Dong L, Yan L, Hou WG, Liu SJ (2010) Synthesis and release behavior of composites of camptothecin and layered double hydroxide. J Solid State Chem 183(8):1811–1816
47. Ho Y-S, Ofomaja AE (2006) Pseudo-second-order model for lead ion sorption from aqueous solutions onto palm kernel fiber. J Hazard Mater 129(1):137–142
48. Sakore S, Chakraborty B (2013) Formulation and evaluation of enalapril maleate sustained release matrix tablets. Int J Pharm 4(1):21–26